



HAL
open science

A molecular determinant of West Nile virus secretion and morphology as a target for viral attenuation

Justine Basset, Julien Burlaud-Gaillard, Maxence Feher, Philippe Roingear, Felix Rey, Nathalie Pardigon

► **To cite this version:**

Justine Basset, Julien Burlaud-Gaillard, Maxence Feher, Philippe Roingear, Felix Rey, et al.. A molecular determinant of West Nile virus secretion and morphology as a target for viral attenuation. Journal of Virology, 2020, 10.1128/JVI.00086-20 . pasteur-02549098

HAL Id: pasteur-02549098

<https://pasteur.hal.science/pasteur-02549098>

Submitted on 21 Apr 2020

HAL is a multi-disciplinary open access archive for the deposit and dissemination of scientific research documents, whether they are published or not. The documents may come from teaching and research institutions in France or abroad, or from public or private research centers.

L'archive ouverte pluridisciplinaire **HAL**, est destinée au dépôt et à la diffusion de documents scientifiques de niveau recherche, publiés ou non, émanant des établissements d'enseignement et de recherche français ou étrangers, des laboratoires publics ou privés.



Distributed under a Creative Commons Attribution 4.0 International License

1 **A molecular determinant of West Nile virus secretion and**
2 **morphology as a target for viral attenuation**

3

4 Justine Basset^{1,2}, Julien Burlaud-Gaillard^{3,4}, Maxence Feher⁵, Philippe Roingeard^{3,4}, Félix A.
5 Rey⁶, Nathalie Pardigon^{1#}

6

7 ¹ Institut Pasteur, Arbovirus Group, Environment and Infectious Risks Unit, Paris, France

8 ² Université Paris Diderot, Sorbonne Paris Cité (Cellule Pasteur), Paris, France

9 ³ Plateforme IBISA de Microscopie Electronique, PST ASB, Université de Tours and CHRU
10 de Tours, Tours, France

11 ⁴ INSERM U1259, Université de Tours and CHRU de Tours, Tours, France

12 ⁵ Laboratory for Urgent Response to Biological Threats, Institut Pasteur, Paris, France

13 ⁶ Institut Pasteur, Structural Virology Unit, Paris, France and CNRS UMR 3569 Virologie,
14 Paris, France

15

16 # Corresponding author: nathalie.pardigon@pasteur.fr

17

18

19 **Running title:** WNV membrane protein as a target for attenuation

20

21

22 **Key words:** West Nile virus, Flavivirus, attenuation, secretion, membrane protein

23

24 **ABSTRACT**

25 West Nile virus (WNV), a member of the *Flavivirus* genus and currently one of the most
26 common arboviruses worldwide, is associated with severe neurological disease in humans. Its
27 high potential to re-emerge and rapidly disseminate makes it a *bona fide* global public health
28 problem. The surface membrane glycoprotein (M) has been associated with *Flavivirus*-
29 induced pathogenesis. Here we identify a key amino acid residue at position 36 of the M
30 protein whose mutation impacts WNV secretion and promotes viral attenuation. We also
31 identified a compensatory site at position M-43 whose mutation stabilizes M-36 substitution
32 both *in vitro* and *in vivo*. Moreover, we find that introduction of the two mutations together
33 confers a full attenuation phenotype and protection against wild-type WNV lethal challenge,
34 eliciting potent neutralizing antibody production in mice. Our study thus establishes the M
35 protein as a new viral target for rational design of attenuated WNV strains.

36

37 **IMPORTANCE**

38 West Nile virus (WNV) is a worldwide (re)emerging mosquito-transmitted *Flavivirus* causing
39 fatal neurological diseases in humans. However, no human vaccine has been yet approved.
40 One of the most effective live-attenuated vaccines was empirically obtained by serial
41 passaging of wild-type yellow fever *Flavivirus*. However, such an approach is not acceptable
42 nowadays and the development of vaccine rationally designed is necessary. Generating
43 molecular infectious clones and mutating specific residues known to be involved in *Flavivirus*
44 virulence is a powerful tool to promote viral attenuation. WNV membrane glycoprotein is
45 thought to carry such essential determinants. Here, we identified two residues of this protein
46 whose substitutions are key to the full and stable attenuation of WNV *in vivo*, most likely
47 through inhibition of secretion and possible alteration of morphology. Applied to other
48 flaviviruses, this approach should help in designing new vaccines against these viruses that
49 are an increasing threat to global human health.

50

51

52

53 **INTRODUCTION**

54 West Nile virus (WNV) is a *Flavivirus* genus member. Most closely related to another genus
55 member, Japanese encephalitis virus (JEV), but also similar to yellow fever virus (YFV), Zika
56 (ZIKV) and dengue (DV) viruses, WNV is one of the most largely widespread neurotropic
57 arthropod-borne viruses, causing severe neurological symptoms and even death (1, 2). Since

58 its first isolation in Uganda in 1937, recurrent and unpredictable WNV outbreaks have been
59 detected in humans throughout the world generating health problems. Despite its global
60 reemergence, however, there is currently neither treatment nor human vaccine available to
61 cure or prevent the disease (1). In the hope of aiding the development of innovative rationally
62 designed vaccines we focused our research on host-WNV molecular interactions and
63 particularly viral particle assembly in the endoplasmic reticulum (ER) of the infected cell.

64 WNV possesses two structural glycoproteins, the membrane protein (M), processed from a
65 precursor protein (prM), and the envelope protein (E) (3). While the E protein mediates
66 interactions between host cellular factors and the virus for attachment and penetration, prM
67 supports E during folding and shields it from causing premature fusion in the acidic secretory
68 pathway (4). As with other flaviviruses, WNV assembly occurs in the endoplasmic reticulum
69 (ER) and requires interactions between prM, E and the nucleocapsid (5, 6). Following
70 assembly, nascent virions bud into the ER lumen and are then translocated to the Golgi
71 apparatus via trafficking vesicles (7). Once in the *trans*-Golgi network (TGN), prM is cleaved
72 by the cellular furin, leading to the release of the pr peptide in the neutral pH extracellular
73 environment and the formation of mature and infectious M-containing virions (8). Although
74 *Flavivirus* assembly mechanisms have been largely investigated (9, 10), it is still unclear how
75 nascent virions engage the host cell secretory pathway in order to exit the ER, reach the TGN,
76 to then be released at the cell surface.

77 The flavivirus prM/M protein was recently shown to carry virulence determinants (11, 12). In
78 the ectodomain of the M protein, the residue 36 (M-36) was suggested to be essential for
79 proper *Flavivirus* viral morphogenesis, although the underlying mechanisms had not been
80 evaluated (11, 13, 14). It has been shown, however, that among the 32 amino acid differences
81 identified between the yellow fever virus vaccine strain 17D (YFV-17D) and the wild-type
82 YFV Asibi strain, there is only one mutation in M at position 36, L36F (15). Noticeably, the
83 same L36F substitution is found in another YFV vaccine strain the French neurotropic virus
84 FNV (16). YFV L36F was shown to be partially responsible for the inability of YFV-17D to
85 infect and disseminate in mosquitoes (14). Interestingly, in other flaviviruses M-36 is always
86 occupied by a hydrophobic residue (Figure 1A): either by isoleucine (WNV, JEV, DV2 and
87 DV4), alanine (DV1 and DV3) or leucine (YFV Asibi), and any substitutions of this M-36
88 residue always lead to a decrease in the production of virus-like-particles (VLPs) in
89 mammalian cells (11, 13, 17). Additionally, we recently demonstrated that in JEV,
90 substitution of isoleucine at M-36 for phenylalanine abolished infectious virus production by
91 altering late steps of the viral cycle (11).

92 As specific recognition signals between cellular and viral components are required for viral
93 particle assembly and egress, we investigated the possible involvement of residue M-36 in
94 WNV assembly and secretion from the ER to the Golgi apparatus. We substituted the
95 isoleucine residue for a phenylalanine at position 36 in the M protein of WNV, generating an
96 attenuated virus that displayed an impaired secretion but that was not stable. We then
97 introduced a sterically compensatory substitution in the same protein at position 43, M-A43G
98 and obtained the stabilized double mutant M- I36F/A43G. This double mutant retained the
99 specificities of the single mutant, eliciting a fully protective immune response against a lethal
100 WT challenge in mice. We thus identified the M-36 residue as a molecular determinant of
101 virulence that is crucial for efficient secretion of newly synthesized virions, and the M-43
102 residue that accommodates and stabilizes a substitution in M-36. Our study strongly suggests
103 that export of newly formed WNV particles from the ER may depend on their morphology
104 and identifies the M protein as a new target for the rational design of attenuated WNV strains
105 to prevent WNV disease.

106

107

108

109

110 **RESULTS**

111

112 **Mutation of M-36 affects WNV infectious cycle by potentially altering the M protein 3-**
113 **dimensional structure**

114 Mirroring the M-L36F mutation in the YFV 17D vaccine, we replaced isoleucine 36 of the
115 WNV M protein with a phenylalanine (M-I36F) (Figure 1B). The resulting mutant virus was
116 successfully produced in C6/36 cells electroporated with genomic RNA synthesized *in vitro*
117 (see Material and Methods) (Figure 1C) and contrary to wild-type WNV, M-I36F mutant
118 displayed a smaller foci phenotype in Vero cells, which is a potential attenuation marker
119 (Figure 1D, M-I36F). Conversely, substitution of the parental isoleucine 36 with an alanine
120 (Figure 1B, M-I36A) did not affect foci size (Figure 1D, M-I36A). More importantly, we
121 observed that only the M-I36F mutation impaired WNV infectious cycle in mammalian
122 neuronal SK-N-SH cells (Figure 1E) suggesting that the nature of residue 36 is essential for
123 efficient viral particle production in these cells. While isoleucine, alanine and phenylalanine
124 possess close chemical properties, only the phenylalanine has an aromatic ring. To examine
125 how M-I36F might physically impact interactions with neighboring amino acids, we mapped
126 either WNV M-I36F or WNV M-I36A into the recently published JEV M protein 4.3Å cryo-
127 EM structure (18), revealing that M-I36F (Figure 1F), but not M-I36A (Figure 1G), clashes
128 with an alanine residue (A43) located in the first transmembrane segment of M (TM1). Thus,
129 while interactions between the two structural proteins E and M are seemingly conserved, M-
130 I36F potentially disrupts the M protein 3-dimensional structure such that steric hindrance is
131 introduced between the phenylalanine aromatic ring and the side chain methyl group of A43.

132

133 **Compensatory mutation partially rescues M-I36F mutant to wild-type phenotype**

134 To compensate the potential clash between the aromatic ring of residue 36 and the side chain
135 of residue 43, we substituted the original A43 by a residue that has no methyl group, namely a
136 glycine (M-A43G) in order to create more space, thereby generating a double mutant virus M-
137 I36F/A43G. We recovered and amplified WNV M-I36F/A43G, M-A43G and wild-type
138 viruses from mosquito C6/36 cells electroporated with genomic RNA synthesized *in vitro*
139 (see Material and Methods). All viruses were found to form large foci on mammalian Vero
140 cells (data not shown), and replicated similarly as assayed for RNA production, in Vero
141 (Figure 2A) and C6/36 cells (Figure 2B), indicating that the M-I36F and M-A43G mutations
142 alone or together did not

143 affect genome decapsidation and replication in mammalian and mosquito cells. When
144 comparing infectious particle production in Vero cell supernatants, however, the titers of M-
145 I36F as well as M-I36F/A43G variants were largely lower than that of wild-type and M-
146 A43G viruses (1.42 logs and 0.93 logs respectively, Figure 2C). Yet the M-I36F/A43G titers
147 were significantly higher than that of M-I36F (Figure 2C). Interestingly, when viruses were
148 grown in C6/36 cells, no difference in titers was observed (Figure 2D). Genetic stability of the
149 mutant viruses was tested by 10 serial passages in Vero cells. Full-genome analysis of M-
150 I36F/A43G passaged up to 10 times revealed the presence of both M-I36F and M-A43G and
151 no other mutation along the genome, while M-I36F alone had already reverted to WT
152 sequence at passage 2 without compensatory mutation elsewhere in the genome (data not
153 shown). A decrease in the amount of genomic viral RNA was observed over time in Vero cell
154 supernatants infected with M-I36F or M-I36F/A43G mutants as compared to wild-type or M-
155 A43G viruses (Figure 2E), that mirrored the decrease in infectious titers in mammalian cells
156 (Figure 2C) and corroborating a decrease in the number of secreted particles. No change in
157 the amount of genomic viral RNA in mosquito cells infected either with wild-type or any
158 mutant viruses was detected (Figure 2F), again reflecting what we observed in terms of titers
159 in these cells (Figure 2D). Interestingly, neither M-I36F nor M-I36F/A43G mutant virus
160 infection of mammalian cells induced any cell death (Figure 2G, Vero cells, and 2H, SK-N-
161 SH cells), contrary to WT and A43G viruses. This result agrees with previous reports
162 showing that residue M-36 can modulate the death-promoting activity of the M protein
163 ectodomain of Flaviviruses (19, 20). No cell death induction was observed for either WT or
164 any mutant viruses in infected C6/36 mosquito cells (data not shown). Altogether, these
165 results indicated that the M-I36F mutation leads to an impaired WNV infectious cycle in
166 mammalian cells, most likely due to the alteration of mutant viral assembly and/or egress, that
167 can be partially rescued and completely stabilized by introduction of a second mutation
168 relieving steric hindrance (M-A43G).

169

170 **M-I36F mutation strongly inhibits WNV efficient secretion**

171 As only a few M-I36F/A43G and M-I36F mutant particles were found in the supernatant of
172 mammalian cells, we wondered whether the M-I36F mutation could interfere with proper
173 budding and/or secretion of the viral particles. We examined mammalian cells infected with
174 the different viruses by electron microscopy (Figure 3). Specific sub-cellular ultrastructural
175 changes associated with the presence of each virus were observed in ultrathin sections of Vero

176 cells infected with either wild-type or mutant viruses (Figure 3, panels A, B, C and D).
177 Relatively few wild-type and M-A43G viral particles were observed within the cells, with the
178 occasional particle found in the ER, indicating that the virions are secreted normally (Figure
179 3A and 3B, arrows). On the other hand, in the same cell type, infection with the M-I36F or
180 M-I36F/A43G virus induced large ER swelling and massive accumulation of newly formed
181 viral particles within the ER and ER-derived vesicles (Figure 3C and 3D, arrows). No such
182 impairment of particle secretion with either mutant was observed in infected mosquito cells
183 (Figure 3E, 3F). Importantly, the M-I36F and M-I36F/A43G mutant particles were released
184 into the ER lumen of the infected mammalian cells and not retained at the ER membrane
185 indicating that assembly and budding steps still occurred in the presence of the M-I36F
186 mutation alone or associated with M-A43G (Figure 3A, 3B, 3C and 3D, zooms). The overall
187 aspect of WNV M-I36F and M-I36F/A43G mutant particles seemed irregular as compared to
188 wild-type and M-A43G mutant viruses in mammalian cells (Figure 3A, 3B, 3C and 3D,
189 zooms), suggesting that WNV morphology was potentially altered by the M-I36F mutation.
190 Indeed, the few secreted M-I36F/A43G virions into the supernatant of mammalian cells at
191 24h pi directly observed by standard negative staining electron microscopy seemed to display
192 an altered morphology although the nucleocapsid and the lipid envelope were still well
193 delineated (Figure 4C). While we were unable to obtain any image for M-I36F mutant due to
194 an insufficient number of secreted particles, that of wild-type and mutant M-A43G virions
195 showed typical characteristics of flavivirus particles (Figure 4A and 4B). The specificity of
196 the particles produced from infected mammalian cells was confirmed using immunogold
197 labeling with mAb 4G2 and the presence of WNV E protein at the surface of wild-type, M-
198 A43G or M-I36F/A43G virions was unambiguously observed (Figure 4D, 4E and 4F),
199 although less labeling was found at the surface of the double mutant virions. On the other
200 hand, wild-type and mutant M-I36F, M-A43G and M-I36F/A43G virions collected from
201 supernatants of mosquito cells all displayed the morphological characteristics of classic
202 flaviviruses (Figure 4G, 4H and 4I). Taken together these data suggest that the M-I36F
203 mutation affects virion secretion possibly by altering WNV morphology only in mammalian
204 cells.

205

206 **Atypical particle morphology of the M-I36F/A43G variant impacts WNV antigenic** 207 **profile**

208 Thus potential modification(s) of M protein structure caused by the M-I36F might lead to
209 altered viral particle morphology with irregularly shaped mutant virions. We reasoned that

210 such atypical morphology of the mutant particles may impact the virion antibody recognition.
211 We therefore first evaluated the recognition profile of wild-type and mutant virions by direct
212 ELISA
213 (Figure 5). While viruses produced in C6/36 cell supernatants are all similarly recognized by
214 the mAb 4G2 that binds specifically the fusion loop of the E protein (21, 22) (Figure 5A),
215 recognition of M-I36F/A43G virus collected in the supernatant of Vero cell is significantly
216 decreased by approximately 1.2-fold for any antibody dilution when compared to wild-type
217 and the M-A43G (Figure 5B). A similar significant decrease (ranging from 1.2 to 2-fold,
218 depending on the antibody dilution) in recognition of WNV M-I36F/A43G produced in Vero
219 cells by mAb 4G2 was obtained using indirect non-competitive ELISA (Figure 5D), while
220 viruses produced in C6/36 cell supernatants are all similarly recognized (Figure 5C).
221 Importantly, no difference in recognition by polyclonal anti-WNV antibody of wild-type and
222 mutant viruses produced either in insect (Figure 5E) or mammalian cells (Figure 5F) was
223 observed, indicating that despite a slight significant decreased recognition of protein E fusion
224 loop, the general antigenic properties of WNV M-I36F/A43G mutant virus are conserved.
225 WNV surface epitopes are essential for both efficient recognition and cell attachment, and the
226 proper folding of the E protein chaperoned by the M protein in the prM-E complex plays a
227 critical role in them. We therefore tested the infectious capacity of our mutant and wild-type
228 viruses under conditions allowing viral binding, but not internalization, to SK-N-SH
229 mammalian cells or C6/36 mosquito cells by evaluating viral genomic RNA associated with
230 the cell surface (Figure 5G and 5H respectively). Comparing viruses produced in mammalian
231 cells and assayed at the surface of SK-N-SH or C6/36 cells, levels of M-I36F/A43G RNA
232 were reduced by around 1-log as compared to that of the wild-type and M-A43G viruses
233 (Figure 5G and 5H), indicating that the WNV double mutant M-I36F/A43G has impaired
234 binding to host cells. Conversely, wild-type, M-I36F, M-A43G and M-I36F/A43G produced
235 in insect cells showed no difference in RNA levels (Figure 5I and 5J). To confirm that the
236 decreased infectious capacity of M-I36F/A43G mutant virus was not simply due to a lack of
237 maturation, we tested for the presence of immature (prM) and mature (M) forms of the
238 membrane glycoprotein at the surface of wild-type or mutant virions collected from Vero cell
239 supernatants by Western Blot (Figure 5K). The presence of similar levels of prM and M for
240 wild-type and mutant viruses alike suggested that all viruses undergo a similar maturation
241 process. Taken together, the above results support the notion that virions harboring the M-
242 I36F mutation have a possible altered morphology, while the main WNV antigenic properties
243 are conserved.

244

245 ***In vivo* effects of WNV M-I36F and/or M-A43G mutations**

246 The *in vitro* properties of WNV M-I36F and M-I36F/A43G mutants encouraged us to test
247 their phenotype *in vivo*. We first assessed pathogenicity in a well-established mouse model of
248 WNV-induced encephalitis (23). In contrast to the high mortality rate observed among mice
249 infected with either wild-type or M-A43G WNV (in which all 15 animals died), only 4 of 15
250 WNV M-I36F-infected mice died after being infected while all mice infected with M-
251 I36F/A43G survived (Figure 6A). As expected, the wild-type, M-A43G and M-I36F-infected
252 mice that died presented rapid weight loss beginning at day 6 pi (Figure 6B, purple, pink and
253 red curves). Conversely, rather than weight loss, we observed normal weight gain among
254 mice that survived the infection (Figure 6B, yellow and green curves). To investigate whether
255 WNV M-I36F and M-I36F/A43G mutants were attenuated due to a less effective viral
256 dissemination, we collected blood samples every other day following the infection, for 10
257 days, and assayed for viral load. The results showed viral loads peaked at day 3 for both the
258 mutants M-A43G and M-I36F/A43G, but slightly later, at day 5pi, for wild-type and the M-
259 I36F mutant (Figure 6C). At day 3 or 5 pi, however, blood viral loads of M-I36F survivors
260 and M-I36F/A43G were 3.4- or 14.7-fold and 4- or 7.6-fold lower, respectively, compared to
261 that of wild-type-infected mice (Figure 6C). Taken together these data indicate that the M-
262 I36F/A43G and M-I36F viruses are rapidly cleared following infection. Sequence analyses of
263 the entire M-I36F/A43G mutant genome collected from blood samples revealed no reversion
264 to wild-type and no compensatory mutation (data not shown). This contrasts dramatically
265 with the results of sequencing M-I36F viral genomes harvested from mice that did not survive
266 the infection, which showed a reversion to the parental genotype (M-I36) (data not shown).
267 Altogether, these results demonstrate that the M-I36F mutation strongly attenuates WNV *in*
268 *vivo* and that the presence of the M-A43G mutation allows for stable retention of M-I36F
269 attenuation without negative impact.

270 Next, we investigated the immunogenic profile of the M-I36F and M-I36F/A43G mutants in
271 mice (Figure 6, panels D and E). A single intraperitoneal injection of either M-I36F or M-
272 I36F/A43G into adult BALB/c mice induced high levels of both WNV-specific IgG and
273 neutralizing antibodies at day 27 post-infection (geometric mean titer = 102.86 and 110
274 respectively, Figure 6D and 6E respectively). Induction of a remarkably robust neutralizing
275 antibody response to WNV M-I36F and M-I36F/A43G in mice led us to explore the
276 protection afforded against a lethal challenge with the wild-type strain. Mice that had survived
277 infection with M-I36F or M-I36F/A43G virus, or control mice injected with PBS, were

278 infected with 1000 FFU of wild-type WNV. Not surprisingly, all but one control mouse
279 developed symptoms upon intraperitoneal challenge and died from the infection around 8
280 days pi. Importantly, none of the mice that had been injected with a single dose of the M-
281 I36F/A43G mutant virus

282 exhibited symptoms after being challenged with wild-type WNV, and all survived the
283 infection (Figure 6F, green curve). Such protection was also conferred to mice that had
284 survived M-I36F mutant infection when the mutant virus did not revert (Figure 6F, yellow
285 curve). These results demonstrate that the M-I36F and M-A43G mutation combination
286 confers both full attenuation of WNV and full protection against wild-type WNV challenge in
287 mice.

288

289

290 **DISCUSSION**

291

292 WNV is one of the most widely distributed arboviruses in the world (24). Responsible for
293 encephalitis in equids and humans, this virus recently re-emerged in Europe during the 2016
294 and 2018 summers, causing an unusual number of human cases, including almost two
295 hundred deaths (25). Currently no treatment or human vaccine is available. We focused our
296 study on one of the two surface glycoproteins, namely the M membrane protein. Previously
297 the M protein has been described as being essential for viral maturation and fusion steps (8).
298 In the present study we now reveal a role for this protein in WNV secretion by demonstrating
299 that a phenylalanine for an isoleucine substitution at position 36 of the M protein (M-I36F)
300 drastically decreases virion secretion out of the mammalian ER to the Golgi apparatus. This
301 substitution appears to perturb the morphology of newly formed virions, which leads to
302 massive ER accumulation of WNV progeny, while the same mutation does not seem to affect
303 the morphology or secretion of virions during mosquito cell infection. We propose that the M-
304 I36F substitution may cause steric hindrance that could directly affects the structure of the M
305 protein. Importantly, in a mouse model of WNV infection, we found that the M-I36F mutant
306 virus is strongly attenuated, resulting in the survival of most of the mice upon infection and
307 all survivors producing neutralizing antibodies. As this mutation is unstable, stochastically
308 reverting to wild-type within the mice, we demonstrate that we could achieve full stabilization
309 of M-I36F by introducing a sterically compensatory substitution in the M protein, M-A43G.
310 We found that this stable double mutant (M-I36F/A43G) retained the specific impaired
311 secretion, viral attenuation, and resultant production of neutralizing antibodies found in the
312 mice infected with the single M-I36F virus.

313

314 **Clash between M-36 and M-43 residues likely affects viral secretion and morphology**

315 Our results indicate that the M-I36F mutation directly affects WNV infectious cycle most
316 likely by causing a clash between the phenylalanine residue and the alanine at position M-43
317 located
318 in TM1. Similarly, substitution of residue M-36 also impairs JEV late steps, DV production
319 and even YFV dissemination (11, 13, 14), suggesting that the nature of the amino acid M-36
320 is crucial for *Flavivirus* particle production. Phenylalanine chemical properties are close to
321 those of the residues mainly found at position M-36 of other flaviviruses (A, I or L).
322 Therefore, its introduction may not change the nature of the M protein helical region.
323 However, introduction of a larger residue at position M-36 could lead to a steric hindrance.
324 Due to its volume, phenylalanine at position 36 might repel the M-A43 residue, that could
325 disturb TM1 alpha helix positioning. M protein TM1 domain is known to be involved in viral
326 assembly and secretion of *Flavivirus* likely through its interaction with TM2 domain (26–28).
327 Interestingly, disruption of JEV TM1/TM2 interactions has been shown to decrease the
328 secretion of JEV virus-like-particles (26). Our observations contend that introduction of a
329 large residue such a phenylalanine at position M-36 is disruptive, while that of a small residue
330 as an alanine is not. By potentially repulsing residue M-43 in TM1, phenylalanine could
331 disturb interactions critical to proper viral biogenesis. We found that a compensatory
332 substitution of the M-A43 residue for a glycine in TM1, a residue that does not have a side
333 chain, partially restores a wild-type phenotype with a significantly greater quantity of viral
334 particles secreted in cell culture supernatants, seemingly by relieving the clash.

335

336 **M-36 residue is crucial for correct virus secretion by potentially altering viral**
337 **morphology**

338 Membrane curvature is known to be essential for *Flavivirus* morphology (29). Because our
339 data potentially associate the M protein with viral morphology, and due to its location at the
340 surface of the particle and its interactions with the ER-derived lipid membrane, it is possible
341 that the M protein ectodomain mutation could directly affect the membrane curvature, thus
342 resulting in abnormal viral budding. It has been shown that *Flavivirus* heterodimers of prM
343 and E assemble laterally and their association induces ER membrane curvature in an isometric
344 network (30). Therefore, introducing an aromatic phenylalanine residue that directly faces the
345 ER membrane could, due to modified hydrophobic interactions, cause partial insertion of the
346 M ectodomain into the ER membrane. As secretion and morphology of the mutant M-I36F
347 and M-I36F/A43G virions from infected mosquito cells are normal, interactions between the
348 M ectodomain and the ER membrane are probably unaffected by the I36F mutation in these

349 cells. Since mosquito cells grow at a lower temperature than mammalian cells (28°C versus
350 37°C), one hypothesis could be that temperature by itself might be responsible for the M-I36F
351 mutant phenotype by

352 affecting viral assembly. However, preliminary data we obtained with WNV M-I36F mutant
353 from mammalian cells cultivated at 32°C show that secretion is still altered as compared to
354 that of wild-type virus (data not shown).

355 We demonstrated that it is the M-I36F mutation alone that causes alteration of WNV
356 infectious cycle, as the M-A43G mutation alone has no effect by itself. Intriguingly, it has
357 been shown that the substitution in DV1 virus-like particles of the M-L36 residue by an
358 alanine increases prM and E glycoproteins interactions, leading to particle condensation (17).
359 Such a condensation may particularly affect the "breathing" of the particles, a dynamic
360 phenomenon dependent on temperature ensuring the metastability of E dimers and transient
361 exposure of this protein's buried domains. Since the WNV M-I36A substitution does not
362 affect the viral cycle, we cannot conclude that such mutation alters or not a dynamic
363 phenomenon of WNV particle "breathing".

364 Our results also indicate a lack of virus-dependent cell death in mammalian cells infected with
365 M-I36F and M-I36F/A43G mutants, contrary to WT and M-A43G viruses. Residue M-36 is
366 located in the pro-apoptotic domain ("apoptoM") of the M protein that was shown to be
367 essential for apoptosis induction by Flaviviruses (19, 20). The M-I36F substitution in the M
368 protein of YFV vaccine strain 17D abolished apoptosis induction, pointing to a crucial role
369 for the M-36 residue. Importantly, the pro-apoptotic activity of M protein ectodomain has
370 been associated with its transport along the secretory pathway and its localization in a post-
371 Golgi compartment (20). The massive accumulation of WNV M-I36F mutants within the ER
372 and the ensuing inhibition of particle secretion that we observed probably hampered the
373 export of the M ectodomain from the Golgi apparatus to the plasma membrane, abolishing
374 apoptosis initiation. Noticeably, introduction of M-A43G mutation in the M-I36F mutant,
375 while partially rescuing WNV life cycle, did not restore death promoting activity.

376

377 **M-I36F and M-A43G mutations together fully attenuate WNV *in vivo***

378 We demonstrate that the altered virulence of our mutant virions drives a strong viral
379 attenuation in a mouse model of WNV-induced encephalitis (23, 31, 32). Although the
380 phenylalanine substitution at position M-36 was naturally selected for in the YFV vaccine
381 strain 17D (15), reducing the ability of the virus to spread in the mosquito (14), the role of
382 this mutation in the mammalian host has yet to be evaluated. The M-36 residue may
383 represent a common virulence factor to *Flavivirus*, however, since it has been demonstrated
384 that introduction of a M-I36F mutation in JEV leads to production of a live attenuated virus in
385 a murine model (11). Although

386 the quick reversion of M-I36F to wild-type underlines the low stability of this mutation when
387 it is alone, the simultaneous presence of M-I36F and M-A43G mutations brings a stability to
388 the resulting virus, without apparent reversion or compensatory mutation during the infection.
389 Thus, the combination of these mutations leads to a double mutant virus with all the
390 characteristics of a fully attenuated virus *in vivo*: suppression of lethality, limited weight loss,
391 weak viremia, no neurological symptoms and production of neutralizing and protective
392 immune response against a lethal challenge.

393 Curiously, the M-I36F mutation slightly alters antibody recognition by 4G2-monoclonal
394 antibody, while the general antigenic properties of WNV M-I36F/A43G mutant virus are
395 conserved (see Figure 5). The mAb 4G2 has been characterized to bind specifically the fusion
396 loop of the E protein (21, 22). As the fusion loop is buried in the E dimer at the particle
397 surface, mAb 4G2 can bind this epitope only when the E dimer dissociates. The M-I36F
398 mutation we introduced may impair the accessibility of the E fusion loop either by masking it
399 or by blocking it in a "buried" state. However, mAb 4G2 can also bind to immature patches in
400 partially mature particles. Interestingly, such partially mature particles are readily found in
401 our cell culture supernatants, as evidenced by the presence of both prM and M proteins in all
402 viruses (Figure 5K). Importantly, the M-I36F mutation, while making virions less infectious,
403 does not alter general antigenic recognition as shown both *in vitro* and *in vivo* (Figure 5F and
404 6D and 6E). Protection against flaviviruses is correlated to a large production of neutralizing
405 antibodies (33–35). Neutralizing antibodies are generally most efficient when directed against
406 a specific amino acid sequence in domain III of the E glycoprotein (36). Our *in vitro* data
407 indicate that M-I36F and M-I36F/A43G mutant viruses have kept highly immunogenic
408 epitopes and these mutations have not altered recognition of this E domain *in vivo*. On the
409 other hand, antibodies directed against the domain II fusion loop of flaviviruses are generally
410 poorly neutralizing, and may lead to an increase in the antibody-dependent enhancement
411 phenomenon (ADE) (37, 38). It would be interesting to evaluate whether the presence of M-
412 I36F et M-A43G mutations, by decreasing recognition of protein E fusion loop, may
413 potentially reduce ADE.

414 Our study provides a robust proof-of-concept that M-I36F/A43G mutations may be used as a
415 platform for the development of rationally-designed attenuated WNV strains. Of course, a
416 vaccine to prevent WNV infection must protect against all genotypes, especially in the view
417 of the recent emergence of lineage 2 neuroinvasive strains in Europe (39). It is known that
418 prM and E proteins of one lineage cross protect against another lineage of WNV (40, 41).
419 Therefore,

420 it would be of interest to test the protective efficacy of our lineage 1 double mutant virus on a
421 circulating strain of lineage 2. Live attenuated vaccines against various virus infections have
422 been empirically obtained by successive passages of wild-type virus strains and therefore may
423 present significant risks of vaccinal accidents. To cope with the spread of *Flavivirus*
424 worldwide, the development of rational vaccine design approaches is inevitable. Our study
425 opens new perspectives for the development of live-attenuated vaccines based on molecular
426 alteration of virulence determinants in viral genomes produced from infectious clones.

427

428

429 MATERIAL AND METHODS

430

431 **Cells**

432 Green monkey epithelial cells (Vero-E6), and human neuroblastoma derived cells (SK-N-SH)
433 were maintained at 37°C in Dulbecco's Modified Eagle Medium (DMEM, Life Technologies)
434 supplemented with 10% of heat-inactivated fetal bovine serum (FBS). *Aedes albopictus* cells
435 C6/36 were maintained at 28°C in Leibovitz medium (L15, Life Technologies) supplemented
436 with 10% of FBS.

437

438 **Production of recombinant WNV**

439 The "two-plasmids" cDNA clone of WNV Israel 1998 strain produced in our lab (31) was
440 used. Mutations M-I36F and/or M-A43G were directly introduced in pUC57-5'UTR-NS1
441 through PCR mutagenesis using primers 5'-
442 AAAACAGAATCATGGTTCTTTGAGGAACCCTGG-3' and 5'-
443 CCAGGGTTCCTCAAGAACCATGATTCTGTTTT-3' (M-I36F) or 5'-
444 ACCCTGGATATGGACTGGTGGCAGC-3' and 5'-
445 GCTGCCACCAGTCCATATCCAGGGT-3' (M-A43G). Mutations are underlined.

446 The production of a full-length infectious clone was performed as already described (31),
447 purified and transcribed *in vitro* using the mMessage mMachine SP6 kit (ThermoFischer
448 Scientific). The resulting RNA was electroporated in C6/36 cells (400 V, 25µF, 800Ω) in
449 OPTI-MEM medium (ThermoFischer Scientific). Cell culture supernatants were collected
450 72h post-electroporation and used to infect 10⁷ C6/36 cells. Three-days pi, viral supernatants
451 were amplified by infecting 5 x 10⁷ C6/36 cells during 3 days before collection and utilization
452 as final viral stocks. Full-length viral genomes were sequenced from cDNA obtained by

453 reverse transcription using Superscript II Reverse Transcription kit (Invitrogen) according to
454 manufacturer's instructions. cDNAs were then amplified by PCR using Phusion High Fidelity

455 kit (ThermoFischer Scientific) and primers presented in Table 1.

456

457 **Antibodies**

458 Monoclonal antibody (mAb) 4G2 anti-*Flavivirus* E protein and HRP-conjugated mAb 4G2
459 were purchased from RD Biotech (Besançon, France). Polyclonal anti-WNV was isolated
460 from intraperitoneal liquid of mice infected with WNV. Secondary antibody Horseradish
461 peroxidase (HRP)-conjugated goat anti-mouse IgG was purchased from Bio-Rad
462 Laboratories. Secondary gold-conjugated goat-anti-mouse antibody was purchased from
463 Aurion (Wageningen, Netherlands).

464

465 **M protein 3-fold structure**

466 M protein 3D structure data were obtained from the PDB (PDB accession number: 5wsn) and
467 edited using PyMOL program.

468

469 **Quantitative RT-PCR**

470 Total RNA were extracted from samples using NucleoSpin RNA (Macherey-Nagel)
471 according to manufacturer's instructions. The RNA standard used for quantitation of WNV
472 copy number was produced as already described (31). The quantitation of a given target RNA
473 was performed using 2µl of RNA and the Power SYBR™ Green RNA-to-CT™ 1-Step
474 (ThermoFisher Scientific) according to manufacturer's instructions. The QuantStudio™ 6
475 Flex Real-Time PCR Instrument 384-well (Thermo Fisher Scientific) was used to measure
476 SYBR green fluorescence with the following program: reverse transcription step at 48°C
477 (30min), followed by an initial PCR activation step at 95°C (10min), 40 cycles of
478 denaturation at 95°C (15s) and annealing at 60°C (30s). Results were analyzed using the CFX
479 Manager software (Bio-Rad). Primers 5'- GCGGCAATATTCATGACAGCC -3' and 5'-
480 CGGGATCTCAGTCTGTAAGTC -3' were used for viral genome quantitation. Target gene
481 expression was normalized to the expression of GAPDH mRNA, measured using the primers
482 5'- GGTCGGAGTCAACGGATTTG -3' and 5'- ACTCCACGACGTACTCAGCG-3' (42).

483

484

485 **Titration**

486 Vero-E6 cells were seeded at 8×10^4 cells per well in 24-well plates and incubated at 37°C for
487 24h. Tenfold dilutions of virus in DMEM were added to the cells and incubated for 1h at
488 37°C. Unadsorbed virus was removed, then 1ml of DMEM supplemented with 1.6%

489 carboxymethyl cellulose (CMC), 10 mM HEPES buffer, 72 mM sodium bicarbonate, and 2%
490 FBS were added to each well, followed by incubation at 37°C for 2 days. The CMC overlay
491 was removed, the cells were washed with PBS and fixed with 4% paraformaldehyde for
492 15min, followed by permeabilization with 0.2% Triton X-100 for 5min. Cells were then
493 washed with PBS and incubated for 1h at room temperature (RT) with anti-E antibody (4G2),
494 followed by incubation with HRP-conjugated anti-mouse IgG antibody. The foci were
495 revealed using the Vector VIP peroxidase substrate kit (Vector Laboratories) according to
496 manufacturer's instructions.

497

498 **Analysis of the secreted particles by negative staining electron microscopy and** 499 **immunogold labeling**

500 The clarified viral supernatant was purified by polyethylene glycol precipitation followed by
501 ultracentrifugation at 50000G, 4°C for 2h (Ultracentrifuge Optima L-100 XP, Beckman) on
502 iodixanol gradient (OptiPrep, Sigma Aldrich). Fractions of interest were then fixed (v/v) with
503 paraformaldehyde 2% (Sigma, St-Louis, MO), 0.1 M phosphate buffer pH 7.2 overnight.
504 Formvar/carbon-coated nickel grids were deposited on a drop of fixed sample during 5 min
505 and rinsed three times with phosphate-buffered saline (PBS). After a single wash with
506 distilled water, the negative staining was then performed with three consecutive contrasting
507 steps using 2% uranyl acetate (Agar Scientific, Stansted, UK), before analysis under the
508 transmission electron microscope (JEOL 1011, Tokyo, Japan).

509 For immunogold labeling, grids coated with the sample were washed and further incubated
510 for 45 min on a drop of PBS containing 1:10 mouse monoclonal antibody against *Flavivirus E*
511 protein (4G2). After 6 washes with PBS, grids were incubated for 45 min on a drop of PBS
512 containing 1:30 gold-conjugated (10 nm) goat-anti-mouse IgG (Aurion, Wageningen,
513 Netherlands). Grids were then washed with 6 drops of PBS, post-fixed in 1% glutaraldehyde,
514 rinsed with 2 drops of distilled water, before being negatively stained and observed under the
515 microscope as described above.

516

517 **Ultrastructural analysis of the infected cells by transmission electron microscopy**

518 24h-infected Vero or C6/36 cells were trypsinized, rinsed once in PBS, and gently
519 resuspended in cold fixation buffer containing paraformaldehyde 4% (Sigma, St-Louis, MO),
520 1% glutaraldehyde (Sigma), 0.1 M phosphate buffer pH 7.3, for 24h. Cells were then placed
521 in a mixture of (1:1) propylene oxide/Epon resin (Sigma) and left overnight in pure resin for
522 samples impregnation. Cells were then embedded in Epon resin (Sigma), and blocks were

523 allowed to polymerize for 48 hours at 60°C. Ultra-thin sections of blocks were obtained with
524 a Leica EM UC7 ultramicrotome (Wetzlar, Germany). Sections were deposited on
525 formvar/carbon-coated nickel grids and stained with 5% uranyl acetate (Agar Scientific), 5%
526 lead citrate (Sigma), and observations were made with a JEOL 1011 transmission electron
527 microscope.

528

529 **Mouse experiments**

530 Three-weeks old female BALB/c mice (Janvier) were housed under pathogen-free conditions
531 in level 3 animal facility and protocols were approved by the Ethic Committee for Control of
532 Experiments in Animals (CETEA) at the Institut Pasteur and declared to the French Ministry
533 under no. 00762.02. Mice were infected intraperitoneally with 50 FFU of either wild-type, M-
534 I36F, M-A43G, or M-I36F/A43G mutated virus in 50µL of DPBS supplemented with 0,2%
535 bovine serum albumin. Mice were followed daily post-injection, survival rate, weight loss and
536 clinical symptoms were monitored. Every two days pi (day 1, 3, 5, 7 and 9) blood samples
537 obtained by puncture at the caudal vein were collected and tested for the presence of viral
538 RNA. Mice that survived the infection were challenged with 1000 FFU of wild-type virus
539 diluted in 50µL of DPBS + 0,2% BSA at day 28 pi. Mice mortality was followed over time.
540 Blood was obtained by puncture at the caudal vein at day 27 pi, collected in tube containing
541 EDTA and serum separated after centrifugation at 4000G, 10 min in order to perform ELISA
542 and seroneutralization assays.

543

544 **Direct ELISA**

545 Viruses were purified by polyethylene glycol precipitation followed by ultracentrifugation at
546 50000G, 4°C for 2h (Ultracentrifuge Optima L-100 XP, Beckman) on iodixanol gradient
547 (OptiPrep, Sigma Aldrich). Fractions of interest were then UV-inactivated. High-binding 96-
548 well plates (Nunc) were coated with 2µg/mL of purified and inactivated viruses in 100µL of
549 PBS-3% milk and 0,5% Tween 20 (PBS-milk-Tween) and incubated overnight at 4°C. Plates
550 were washed five times with PBS containing 0,05% Tween 20. mAb 4G2, polyclonal anti-
551 WNV antibodies, or sera obtained from mice blood were serially diluted 10-fold (morphology
552 analyses) or 2-fold (mice experiments) starting at 1:100 dilution in PBS-milk-Tween, added
553 to plates and incubated 1h at 41°C. After washing, plates were incubated with 100µL of HRP-
554 conjugated goat anti-mouse IgG diluted 1:10 000 in PBS-milk-Tween for 1h at 41°C. Plates
555 were washed again and 200µL of SIGMAFAST™ OPD (Sigma) substrate was added per well
556 for 30min following manufacturer's instructions. Luminescence was read on plate reader

557 EnVision™ 2100 Multilabel Reader (PerkinElmer, Santa Clara, CA, USA) at a wavelength
558 of 450nm.

559

560 **Indirect ELISA**

561 High-binding 96-well plates (Nunc) were coated with 5µg/mL of polyclonal anti-WNV
562 antibody in 100µL of PBS-milk-Tween and incubated overnight at 4°C. Plates were washed
563 five times with PBS containing 0,05% Tween 20 and 2µg/mL of purified and inactivated
564 viruses were added to plates and incubated 2h at 41°C. After washing, 100µL of HRP-
565 conjugated mAb 4G2 serially diluted 10-fold in PBS-milk-Tween were added to plates and
566 incubated 1h at 41°C. Plates were washed and 200iL of HRP substrate, SIGMAFAST™ OPD
567 (Sigma), was added per well for 30min following manufacturer's instructions. Luminescence
568 was read on plate reader EnVision™ 2100 Multilabel Reader (PerkinElmer, Santa Clara,
569 CA, USA) at a wavelength of 450nm.

570

571 **Seroneutralization assay**

572 Serum samples were two-fold serially diluted in DMEM, with a starting dilution of 1:20.
573 Each dilution was incubated with 50 FFU of wild-type WNV for 1h, under agitation, at 37°C.
574 The remaining viral infectivity was evaluated by FFA on Vero-E6 cells. Sera collected from
575 DPBS-injected mice served as negative controls. Neutralization curves were obtained and
576 analyzed using GraphPad Prism 6 software. Nonlinear regression fitting with sigmoidal dose
577 response was used to determine the dilution of serum that reduced the quantity of FFU by
578 50%.

579

580 **Statistical analysis**

581 Statistical analyses were performed using GraphPad Prism software. Non-parametric Mann-
582 Whitney test was used to compared quantitative data and log-rank (Mantel-Cox) analysis was
583 used for survival data analysis.

584

585

586 **ACKNOWLEDGMENTS**

587 We thank Drs François-Loïc Cosset and Solène Denolly for the protein trafficking
588 experiments and Dr. Jonathan Bradley for critical reading of the manuscript. Financial support
589 was provided in part by Institut Carnot-Pasteur Microbes and Health.

590

591

592 **AUTHORS CONTRIBUTION**

593 Each named author has substantially contributed to conducting the underlying research and
594 drafting this manuscript. Additionally, to the best of our knowledge, none have any conflict of
595 interest, financial or otherwise. J.B., N.P. and P.R. designed the experiments. J.B., M.F. and
596 J.B.G. performed the experiments. F.R. and J.B. conducted the structural analysis. J.B. and
597 N.P. wrote the paper.

598

599

REFERENCES

- 600 1. Chancey C, Grinev A, Volkova E, Rios M. 2015. The Global Ecology and Epidemiology
601 of West Nile Virus. *BioMed Research International* 2015:1–20.
- 602 2. Londono-Renteria B, Colpitts TM. 2016. A Brief Review of West Nile Virus Biology.
603 *Methods Mol Biol* 1435:1–13.
- 604 3. Kuhn RJ, Zhang W, Rossmann MG, Pletnev SV, Corver J, Lenches E, Jones CT,
605 Mukhopadhyay S, Chipman PR, Strauss EG, Baker TS, Strauss JH. 2002. Structure of dengue
606 virus: implications for flavivirus organization, maturation, and fusion. *Cell* 108:717–725.
- 607 4. Zhang Y, Corver J, Chipman PR, Zhang W, Pletnev SV, Sedlak D, Baker TS, Strauss JH,
608 Kuhn RJ, Rossmann MG. 2003. Structures of immature flavivirus particles. *EMBO J* 22:2604–
609 2613.
- 610 5. Mukhopadhyay S, Kuhn RJ, Rossmann MG. 2005. A structural perspective of the
611 flavivirus life cycle. *Nat Rev Microbiol* 3:13–22.
- 612 6. Pryor MJ, Azzola L, Wright PJ, Davidson AD. 2004. Histidine 39 in the dengue virus
613 type 2 M protein has an important role in virus assembly. *J Gen Virol* 85:3627–3636.
- 614 7. Welsch S, Miller S, Romero-Brey I, Merz A, Bleck CKE, Walther P, Fuller SD, Antony C,
615 Krijnse-Locker J, Bartenschlager R. 2009. Composition and Three-Dimensional Architecture
616 of the Dengue Virus Replication and Assembly Sites. *Cell Host & Microbe* 5:365–375.
- 617 8. Yu I-M, Zhang W, Holdaway HA, Li L, Kostyuchenko VA, Chipman PR, Kuhn RJ,
618 Rossmann MG, Chen J. 2008. Structure of the Immature Dengue Virus at Low pH Primes
619 Proteolytic Maturation. *Science* 319:1834–1837.
- 620 9. Apte-Sengupta S, Sirohi D, Kuhn RJ. 2014. Coupling of replication and assembly in
621 flaviviruses. *Current Opinion in Virology* 9:134–142.
- 622 10. Murray CL, Jones CT, Rice CM. 2008. Architects of assembly: roles of Flaviviridae non-
623 structural proteins in virion morphogenesis. *Nature Reviews Microbiology* 6:699–708.
- 624 11. de Wispelaere M, Khou C, Frenkiel M-P, Desprès P, Pardigon N. 2016. A Single Amino
625 Acid Substitution in the M Protein Attenuates. *Journal of Virology* 90:2676–2689.
- 626 12. Yuan L, Huang X-Y, Liu Z-Y, Zhang F, Zhu X-L, Yu J-Y, Ji X, Xu Y-P, Li G, Li C, Wang H-J,
627 Deng Y-Q, Wu M, Cheng M-L, Ye Q, Xie D-Y, Li X-F, Wang X, Shi W, Hu B, Shi P-Y, Xu Z, Qin C-
628 F. 2017. A single mutation in the prM protein of Zika virus contributes to fetal microcephaly.
629 *Science* 358:933–936.
- 630 13. Hsieh S-C, Zou G, Tsai W-Y, Qing M, Chang G-J, Shi P-Y, Wang W-K. 2011. The C-
631 terminal helical domain of dengue virus precursor membrane protein is involved in virus
632 assembly and entry. *Virology* 410:170–180.
- 633 14. McElroy KL, Tsetsarkin KA, Vanlandingham DL, Higgs S. 2006. Role of the yellow fever
634 virus structural protein genes in viral dissemination from the *Aedes aegypti* mosquito
635 midgut. *J Gen Virol* 87:2993–3001.
- 636 15. Monath TP. 2005. Yellow fever vaccine. *Expert Review of Vaccines* 4:553–574.
- 637 16. Wang E, Ryman KD, Jennings AD, Wood DJ, Taffs F, Minor PD, Sanders PG, Barrett
638 ADT. 1995. Comparison of the genomes of the wild-type French viscerotropic strain of
639 yellow fever virus with its vaccine derivative French neurotropic vaccine. *Journal of General*
640 *Virology* 76:2749–2755.
- 641 17. Hsieh S-C, Wu Y-C, Zou G, Nerurkar VR, Shi P-Y, Wang W-K. 2014. Highly conserved
642 residues in the helical domain of dengue virus type 1 precursor membrane protein are
643 involved in assembly, precursor membrane (prM) protein cleavage, and entry. *J Biol Chem*
644 289:33149–33160.
- 645 18. Wang X, Li S-H, Zhu L, Nian Q-G, Yuan S, Gao Q, Hu Z, Ye Q, Li X-F, Xie D-Y, Shaw N,

- 646 Wang J, Walter TS, Huiskonen JT, Fry EE, Qin C-F, Stuart DI, Rao Z. 2017. Near-atomic
647 structure of Japanese encephalitis virus reveals critical determinants of virulence and
648 stability. *Nat Commun* 8:14.
- 649 19. Brabant M, Baux L, Casimir R, Briand JP, Chaloin O, Porceddu M, Buron N, Chauvier D,
650 Lassalle M, Lecoeur H, Langonné A, Dupont S, Déas O, Brenner C, Rebouillat D, Muller S,
651 Borgne-Sanchez A, Jacotot E. 2009. A flavivirus protein M-derived peptide directly
652 permeabilizes mitochondrial membranes, triggers cell death and reduces human tumor
653 growth in nude mice. *Apoptosis* 14:1190–1203.
- 654 20. Catteau A, Kalinina O, Wagner M-C, Deubel V, Courageot M-P, Desprès P. 2003.
655 Dengue virus M protein contains a proapoptotic sequence referred to as ApoptoM. *J Gen
656 Virol* 84:2781–2793.
- 657 21. Crill WD, Chang G-JJ. 2004. Localization and characterization of flavivirus envelope
658 glycoprotein cross-reactive epitopes. *J Virol* 78:13975–13986.
- 659 22. Summers PL, Cohen WH, Ruiz MM, Hase T, Eckels KH. 1989. Flaviviruses can mediate
660 fusion from without in *Aedes albopictus* mosquito cell cultures. *Virus Research* 12:383–392.
- 661 23. Lucas M, Frenkiel M-P, Mashimo T, Guénet J-L, Deubel V, Desprès P, Ceccaldi P-E.
662 2004. The Israeli strain IS-98-ST1 of West Nile virus as viral model for West Nile encephalitis
663 in the Old World. *Virology Journal* 1:9–9.
- 664 24. Kramer LD, Styer LM, Ebel GD. 2008. A global perspective on the epidemiology of
665 West Nile virus. *Annu Rev Entomol* 53:61–81.
- 666 25. ECDC. 2018. West Nile fever in Europe in 2018 - human and equine cases; updated 9
667 November.
- 668 26. Lin Y-J, Peng J-G, Wu S-C. 2010. Characterization of the GXXXG motif in the first
669 transmembrane segment of Japanese encephalitis virus precursor membrane (prM) protein.
670 *Journal of Biomedical Science* 17:39.
- 671 27. Op De Beeck A, Rouillé Y, Caron M, Duvet S, Dubuisson J. 2004. The transmembrane
672 domains of the prM and E proteins of yellow fever virus are endoplasmic reticulum
673 localization signals. *J Virol* 78:12591–12602.
- 674 28. Op De Beeck A, Molenkamp R, Caron M, Ben Younes A, Bredenbeek P, Dubuisson J.
675 2003. Role of the transmembrane domains of prM and E proteins in the formation of yellow
676 fever virus envelope. *J Virol* 77:813–820.
- 677 29. Zhang X, Ge P, Yu X, Brannan JM, Bi G, Zhang Q, Schein S, Zhou ZH. 2013. Cryo-EM
678 structure of the mature dengue virus at 3.5-Å resolution. *Nat Struct Mol Biol* 20:105–110.
- 679 30. Leier HC, Messer WB, Tafesse FG. 2018. Lipids and pathogenic flaviviruses: An
680 intimate union. *PLOS Pathogens* 14:e1006952.
- 681 31. Alsaleh K, Khou C, Frenkiel M-P, Lecollinet S, Vázquez A, de Arellano ER, Desprès P,
682 Pardigon N. 2016. The E glycoprotein plays an essential role in the high pathogenicity of
683 European–Mediterranean IS98 strain of West Nile virus. *Virology* 492:53–65.
- 684 32. Bahuon C, Desprès P, Pardigon N, Panthier J-J, Cordonnier N, Lowenski S, Richardson
685 J, Zientara S, Lecollinet S. 2012. IS-98-ST1 West Nile virus derived from an infectious cDNA
686 clone retains neuroinvasiveness and neurovirulence properties of the original virus. *PLoS
687 ONE* 7:e47666.
- 688 33. Ben-Nathan D, Lustig S, Tam G, Robinzon S, Segal S, Rager-Zisman B. 2003.
689 Prophylactic and therapeutic efficacy of human intravenous immunoglobulin in treating
690 West Nile virus infection in mice. *J Infect Dis* 188:5–12.
- 691 34. Diamond MS, Shrestha B, Marri A, Mahan D, Engle M. 2003. B Cells and Antibody Play
692 Critical Roles in the Immediate Defense of Disseminated Infection by West Nile Encephalitis

- 693 Virus. *Journal of Virology* 77:2578–2586.
- 694 35. Gould LH, Sui J, Foellmer H, Oliphant T, Wang T, Ledizet M, Murakami A, Noonan K,
695 Lambeth C, Kar K, Anderson JF, de Silva AM, Diamond MS, Koski RA, Marasco WA, Fikrig E.
696 2005. Protective and therapeutic capacity of human single-chain Fv-Fc fusion proteins
697 against West Nile virus. *J Virol* 79:14606–14613.
- 698 36. Beasley DWC, Barrett ADT. 2002. Identification of Neutralizing Epitopes within
699 Structural Domain III of the West Nile Virus Envelope Protein. *Journal of Virology* 76:13097–
700 13100.
- 701 37. Thomas S, Redfern JB, Lidbury BA, Mahalingam S. 2006. Antibody-dependent
702 enhancement and vaccine development. *Expert Rev Vaccines* 5:409–412.
- 703 38. Throsby M, Geuijen C, Goudsmit J, Bakker AQ, Korimbocus J, Kramer RA, Clijsters-van
704 der Horst M, de Jong M, Jongeneelen M, Thijsse S, Smit R, Visser TJ, Bijl N, Marissen WE,
705 Loeb M, Kelvin DJ, Preiser W, ter Meulen J, de Kruif J. 2006. Isolation and characterization of
706 human monoclonal antibodies from individuals infected with West Nile Virus. *J Virol*
707 80:6982–6992.
- 708 39. Hernández-Triana LM, Jeffries CL, Mansfield KL, Carnell G, Fooks AR, Johnson N. 2014.
709 Emergence of west nile virus lineage 2 in europe: a review on the introduction and spread of
710 a mosquito-borne disease. *Front Public Health* 2:271.
- 711 40. Martina BE, Koraka P, van den Doel P, van Amerongen G, Rimmelzwaan GF,
712 Osterhaus ADME. 2008. Immunization with West Nile virus envelope domain III protects
713 mice against lethal infection with homologous and heterologous virus. *Vaccine* 26:153–157.
- 714 41. McDonald WF, Huleatt JW, Foellmer HG, Hewitt D, Tang J, Desai P, Price A, Jacobs A,
715 Takahashi VN, Huang Y, Nakaar V, Alexopoulou L, Fikrig E, Powell TJ. 2007. A West Nile virus
716 recombinant protein vaccine that coactivates innate and adaptive immunity. *J Infect Dis*
717 195:1607–1617.
- 718 42. Breiman A, Grandvaux N, Lin R, Ottone C, Akira S, Yoneyama M, Fujita T, Hiscott J,
719 Meurs EF. 2005. Inhibition of RIG-I-Dependent Signaling to the Interferon Pathway during
720 Hepatitis C Virus Expression and Restoration of Signaling by IKK. *Journal of Virology* 79:3969–
721 3978.
- 722

723 **LEGENDS:**

724

725 **Figure 1: The nature of M-36 residue impacts WNV infectious cycle by potentially**
726 **disrupting the M protein 3-dimensional structure.**

727 (A): Sequence comparison of M protein ectodomain and TM1 from different *Flavivirus*.
728 Residue 36 location is indicated in red and that of residue 43 in blue. DV4 accession number
729 MK506266.1, DV2 accession number MK506264.1, DV1 accession number MK506262.1,
730 DV3 accession number MK506265.1, YFV Asibi strain accession number AY640589, YFV
731 17D strain accession number MN708489.1, Zika virus accession number MG827392.1, WNV
732 accession number AF481864.1 and JEV accession number KF907505.1. (B): WNV
733 membrane protein precursor (prM) organization showing ectodomain (ectoM) and part of
734 transmembrane domain 1 (TM1) sequences. Residue at position 36 is indicated in red for WT
735 virus, black for M-I36F or grey M-I36A mutant viruses. (C): Viral stocks were collected from
736 C6/36 cell supernatants at times indicated and titrated by foci-forming assay (FFA) in Vero
737 cells. No statistical difference was observed. (D): Foci morphology of wild-type WNV, M-
738 I36F and M-I36A mutated viral stocks collected from C6/36 supernatants, observed on Vero
739 cells. Vero cells were infected with the indicated virus and foci were observed 48h pi. (E):
740 Growth curves of wild-type, M-I36F and M-I36A mutant WNV. SK-N-SH cells were
741 infected with the indicated virus at a MOI of 1, cell supernatants were collected at indicated
742 times for quantitation of virus titers by FFA using Vero cells. (F): Structure of M-E mature
743 heterodimers (PDB accession number 5wsn). The insert zooms into the A43-F36 contact,
744 with F36 highlighted in pink and A43 in green. The F36 aromatic ring clashes (in red) with
745 the side chain of the A43 located in the TMD-1. (G): Same as (H) with alanine at position M-
746 36. The insert zooms into the A36-A43 contact, with A36 highlighted in pink and A43 in
747 green. No clash between A36 and A43 was observed. The image was generated using
748 PyMOL. The data are representative of 3 independent experiments and error bars indicate
749 standard deviation (SD). * p-value < 0.05; ** p-value < 0.01, *** p-value < 0.001.

750

751

752 **Figure 2: Phenotypical characterization of WNV M-I36F and/or M-A43G mutant**
753 **viruses *in vitro***

754 (A, B): Viral stocks of WNV wild-type and mutants M-A43G, M-I36F and M-I36F/A43G
755 were used at a MOI of 1 to infect (A): Vero cells or (B): C6/36 cells. At the indicated time
756 points, cells were harvested and levels of WNV genomic RNA were quantified by RT-qPCR.

757 **(C, D, E, F):** Growth curves and genome quantitation of wild-type, M-I36F, M-A43G and M-
758 I36F/A43G mutated WNV produced in Vero cells. Vero **(C, E)** and C6/36 cells **(D, F)** were
759 infected with the indicated viruses at a MOI of 1, cell supernatants were collected at indicated
760 times for quantitation of virus titers by FFA using Vero cells **(C, D)** or genome quantitation
761 by RT-qPCR **(E, F)**. **(G, H):** Cell viability. Vero **(G)** or SK-N-SH **(H)** cells were infected
762 with the indicated viruses at a MOI of 1, cells were harvested at indicated times, cell viability
763 was evaluated using CellTiter Glo and represented as a percentage of non-infected control
764 cells. The data are representative of 3 independent experiments and error bars indicate
765 standard deviation (SD). * p-value < 0.05; ** p-value < 0.01, *** p-value < 0.001.

766

767

768 **Figure 3: M-I36F and M-I36F/A43G mutant particles are retained within the ER lumen**
769 **of infected mammalian cells but not in mosquito cells.**

770 **(A, B, C, D, E):** Vero cells were infected with wild-type or mutated WNV in positions M-36
771 and/or M-43 at a MOI of 10 and examined by transmission electron microscopy at 24h pi.

772 **(A):** Vero cells infected with WNV WT. **(B):** Vero cells infected with mutated virus M-
773 A43G. **(C):** Vero cells infected with mutated virus M-I36F. **(D):** Vero cells infected with
774 double mutant virus M-I36F/A43G. **(E, F):** Mosquito C6/36 cells were infected with wild-
775 type or mutated WNV in positions M-36 and/or M-43 at a MOI of 10 and examined by
776 transmission electron microscopy at 24h pi. **(E):** C6/36 cell infected with WNV WT. **(F):**
777 Same with double mutant virus M-I36F/A43G. Examples of viral particles located in the ER
778 lumen are indicated by arrows. Inset bars: 100 nm.

779

780 **Figure 4: Secreted mutant virions M-I36F/A43G display an altered morphology only**
781 **when produced in mammalian cells.**

782 **(A, B, C, D, E, F):** Wild-type and mutated viral particles collected from supernatants of Vero
783 cells infected at a MOI of 10 for 24h, were concentrated and purified. **(A, B, C):** Particles
784 were stained negatively with uranyl and observed by transmission electron microscopy. **(A):**
785 WNV WT particles. **(B):** WNV M-A43G particles. **(C):** WNV M-I36F/A43G particles. **(D, E,**
786 **F):** Viral particles were labeled by immunogold with an anti-protein E pan-flavivirus antibody
787 (mAb 4G2) and observed by transmission electron microscopy. **(D):** WNV WT particles. **(E):**
788 WNV M-A43G particles. **(F):** WNV M-I36F/A43G particles. **(G, H, I):** Wild-type and
789 mutated viral particles collected from supernatants of C6/36 cells infected at a MOI of 10 for
790 24h, were concentrated and purified. Particles were stained negatively with uranyl and

791 observed by transmission electron microscopy. **(G):** WNV WT particles. **(H):** WNV M-A43G
792 particles. **(I):** WNV M-I36F/A43G particles. Bars = 100nm

793

794 **Figure 5: M-I36F mutation effects on WNV antigenic profile.**

795 **(A, B):** Wild-type and mutated WNV surface epitope exhibition was analyzed by direct
796 ELISA. 200ng of different UV-inactivated viruses collected from C6/36 cells **(A)** or Vero
797 cells **(B)** were coated and tested with increasing concentrations of mAb 4G2. **(C, D):** Same as
798 **(A)** and **(B)** using indirect non-competitive ELISA. **(E, F):** Same as **(A)** and **(B)** but with
799 increasing concentrations of polyclonal anti-WNV antibodies. **(G, H):** Infectious capacity of
800 mutant virus M-I36F/A43G is impaired when the virus is produced in mammalian cells. SK-
801 N-SH and C6/36 cells were placed at 4°C for 1h, then infected at a MOI (amount of viral
802 genomic RNA) of 10 for 1h at 4°C with the indicated viruses produced in mammalian cells.
803 **(G):** SK-N-SH cells were collected and viral genomes attached to the cell-surface were
804 quantified by RT-qPCR. **(H):** Same as **(G)** with C6/36 cells. **(I, J):** Infectious capacity of
805 WNV mutated at position M-I36F alone or associated with M-A43G is not affected when the
806 virus is produced in mosquito cells. SK-N-SH and C6/36 cells were placed at 4°C for 1h, then
807 infected at a MOI (amount of viral genomic RNA) of 10 for 1h at 4°C with the indicated
808 viruses produced in mosquito cells. **(I):** SK-N-SH cells were collected and viral genomes
809 attached to the cell-surface were quantified by RT-qPCR. **(J):** Same as **(I)** with C6/36 cells.
810 **(K):** Levels of E, immature prM and mature M glycoproteins were tested under denaturing
811 conditions by Western Blot using a polyclonal anti-WNV antibody. The same amount of viral
812 RNA was loaded in each well. The histograms indicate the median value and the interquartile
813 range determined from triplicate of three independent experiments. *p-value <0.05; ** p-
814 value <0.01; *** p-value <0.001.

815

816 **Figure 6: Combined M-I36F and M-A43G mutations highly attenuate WNV and elicit**
817 **WNV-specific humoral response in a mouse model.**

818 **(A):** Survival curves of 3-weeks-old BALB/c mice inoculated with 50 FFU of the indicated
819 viruses by i.p. route. **(B):** Mice growth curve. Mice weight was measured every day pi and is
820 represented as a percentage of the starting body weight. **(C):** Viral load in mice blood. Viral
821 RNA loads were quantified by RT-qPCR. Dotted line indicates detection limit. **(D, E):** WNV
822 specific-IgG and neutralizing antibodies were measured by ELISA and PRNT₅₀ respectively.
823 **(F):** Survivor mice were challenged with 1000 FFU of wild-type WNV at day 28 pi. Mice
824 were monitored for clinical symptoms and mortality for 25 days. The data are representative

825 of at least two independent experiments and error bars indicate the SD. (* p-value < 0.05; **
826 p-value < 0.01, *** p-value < 0.001).

827

828

829 **TABLE:**

Oligo Forward	Forward Sequence	Tm	Oligo reverse	Reverse Sequence	Tm	Size
11-32F	ctgtgtgagctgacaaacttag	55	780-797R	caagcccccttcttgttc	58	787
501-520F	gacggtaaatgctactgacg	56	1282-1300R	ttcctttgccaatagtc	55	800
1000-1018F	ttggaaggagtgtctggag	56	1781-1800R	agtgttgctgaaaattcca	56	801
1500-1520F	aaagcttggagaatatggaga	56	2278-2295R	atggacagcctccaac	58	796
2000-2017F	cattgaacgacctaacgc	55	2766-2783R	gtgaggcgtttagggtct	56	784
2500-2519F	caagagctgagatgtggaag	56	3281-3298R	agtcaatctctaccggc	55	799
3001-3022F	gaatgtgactcgaagtcattg	57	3777-3799R	ccaccataaacactggtgtatc	58	799
3501-3518F	cctcgtgcagtcacaagt	56	4280-4297R	caatgtcaagctctcca	57	797
4000-4017F	ctagccctgctaaccacc	56	4781-4798R	cctctccgctcatcaaag	57	799
4500-4519F	ttggaagatatggatgctca	57	5277-5294R	acaacctggttggtct	59	795
5003-5020F	ccactggaacatcaggct	57	5783-5800R	ttgggtactccgtctcgt	57	798
5500-5520F	gcaagaggttacattccaca	58	6282-6299R	cacctccggtcgtggtat	59	800
6001-6018F	agaaatccgtcgcaagtt	56	6783-6800R	gagagcagcaacattccg	58	800
6503-6520F	tgcttgagcacttcatgg	59	7283-7300R	aaccgggaacctgtagg	58	798
7031-7049F	caacagcctggtcactgta	55	7775-7792R	agcgatcgacttcgatga	58	762
7500-7517F	acgagaagccggaatttt	57	8255-8275R	ggagcagctccatctctcta	59	776
8000-8017F	gtcccggacatgaagagc	59	8663-8681R	catggttttgagaggacc	58	682
8482-8499F	ggaaaaccctgctcaac	58	9283-9300R	ccagccagctgtgtcatc	59	819
9017-9034F	ggggggaatgtcacactt	58	9782-9800R	tcataccatccagttgacg	55	784
9500-9517F	ttgtcacctacgcctaa	55	10282-10300R	ggttgatagccacctgcat	57	801
10002-10019F	aagagacctgcggctcat	58	10783-10800R	tttcgcctggttaaacac	57	799
10504-10521F	aaagtcaggccgggaagt	60	11011-11028R	atcctgtgtctcgcacc	57	525

830 **Table 1:** Primers used for the amplification and sequencing of the complete wild-type and
831 mutant viral genomes.

832

Figure 1 :

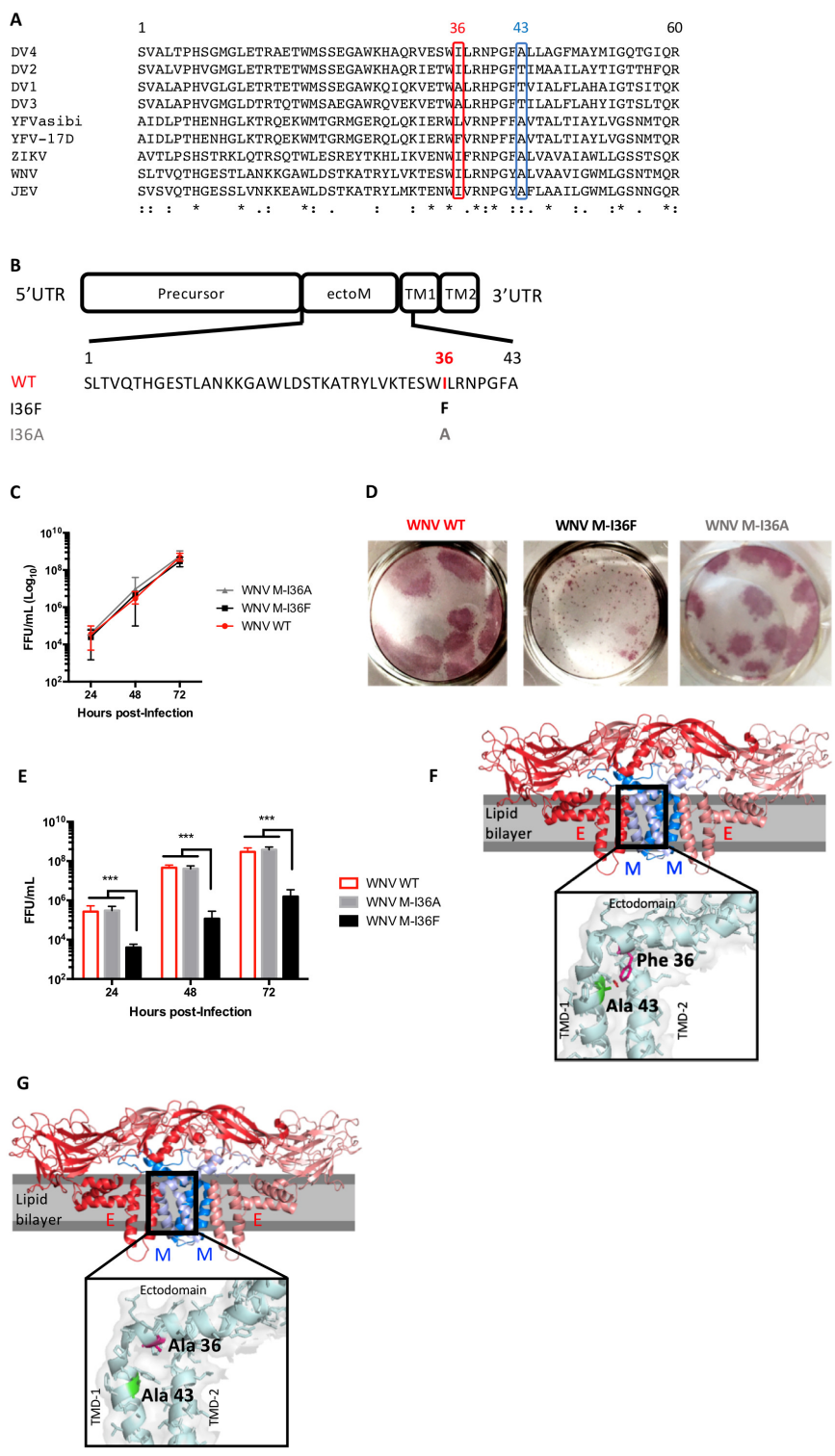
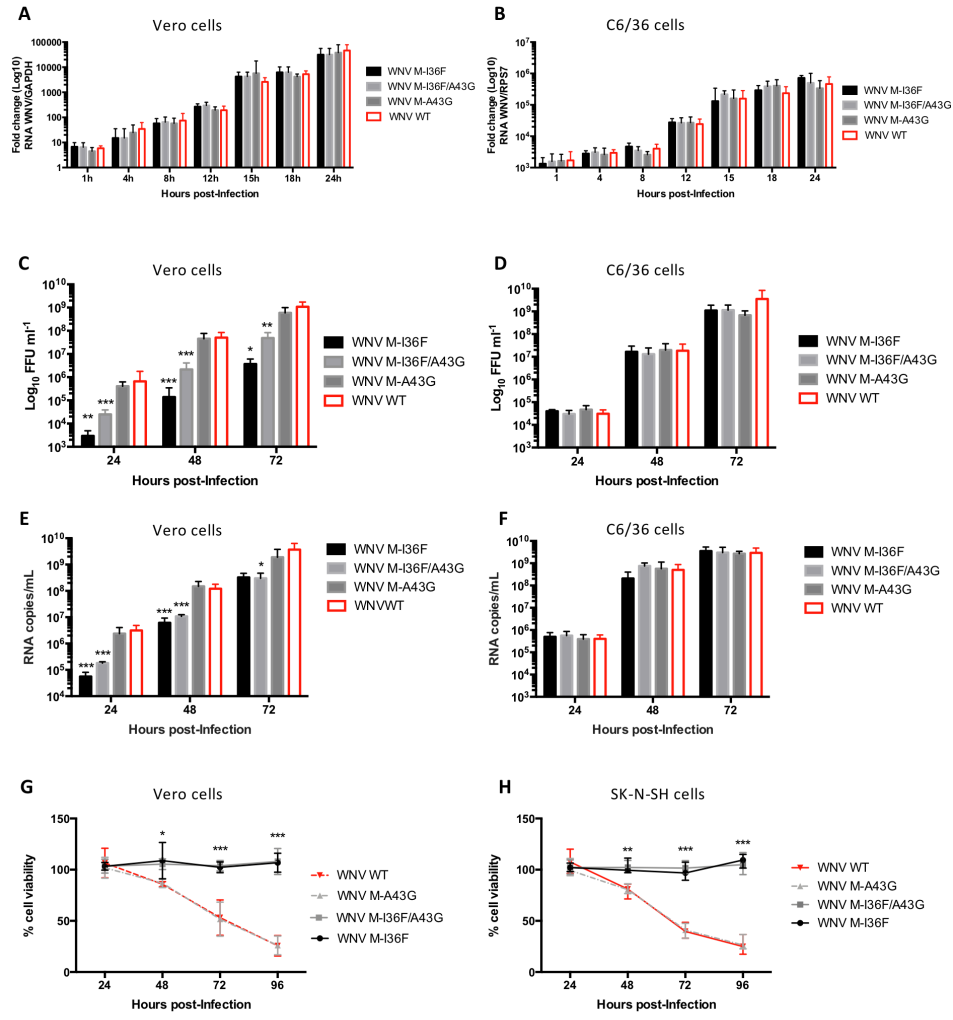
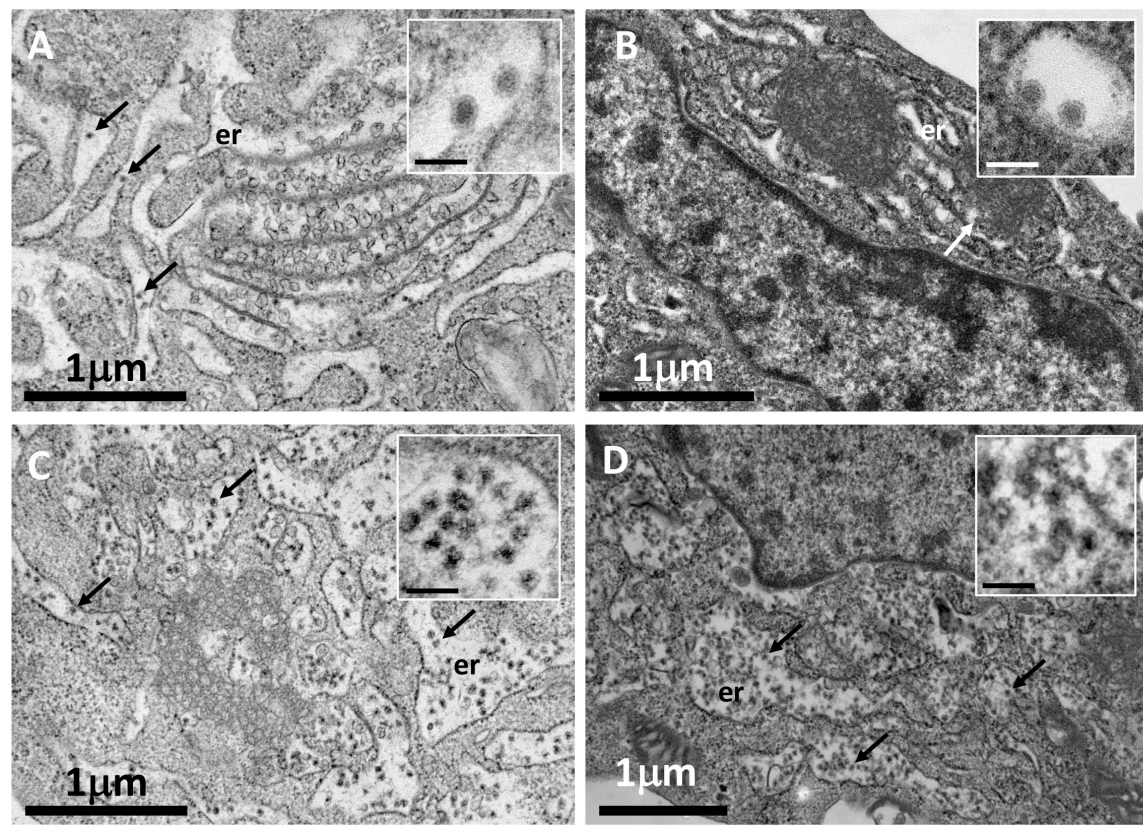


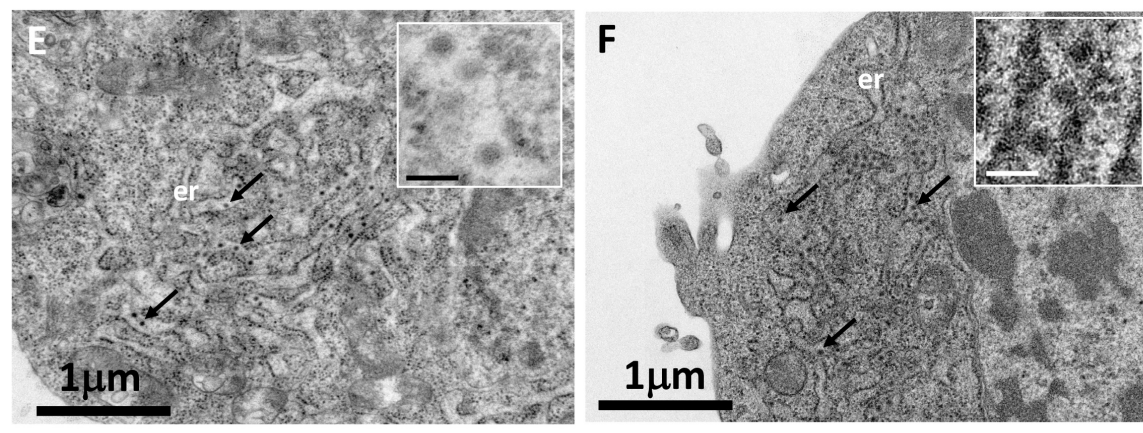
Figure 2:



Vero cells



C6/36 cells



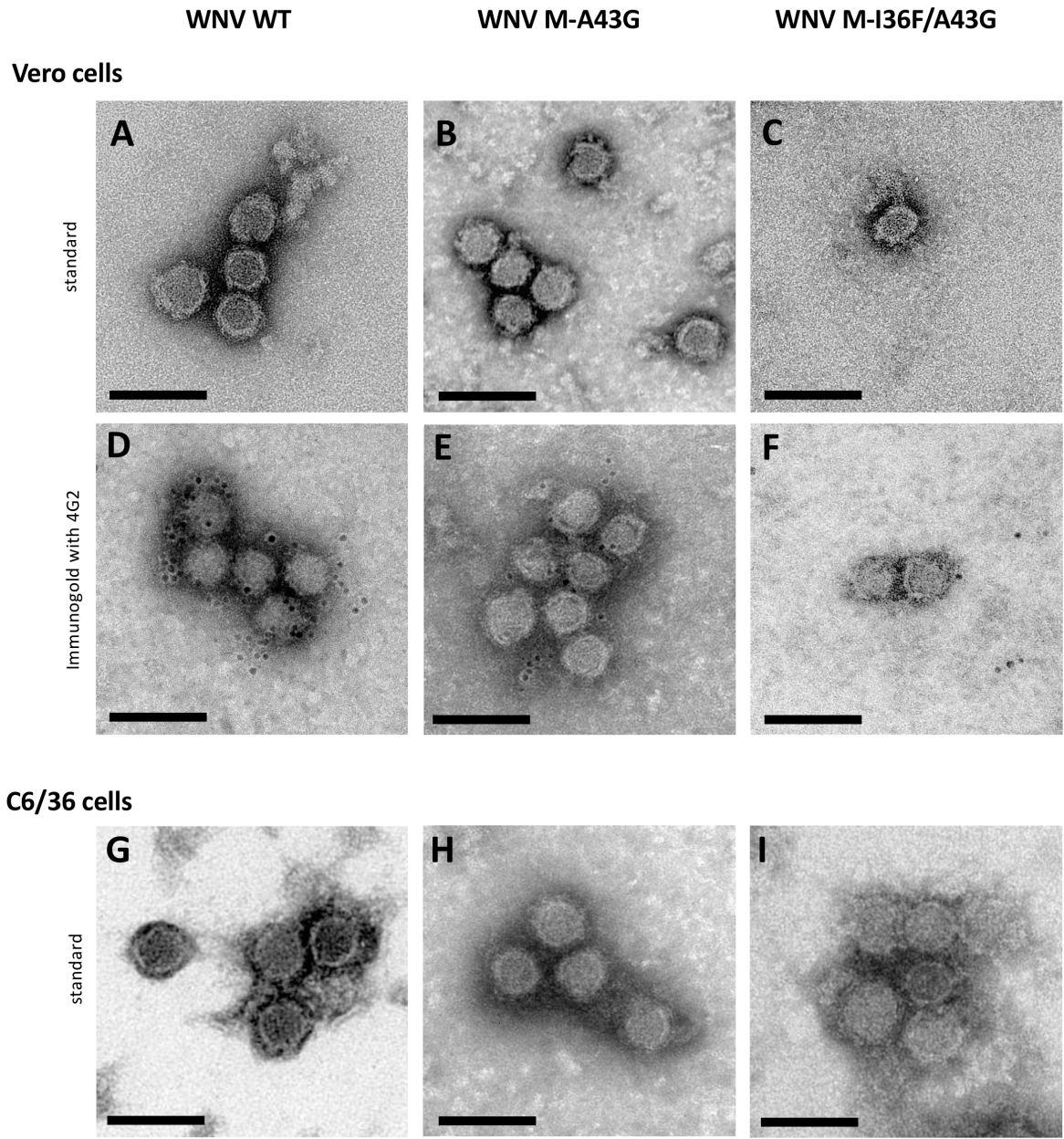


Figure 5:

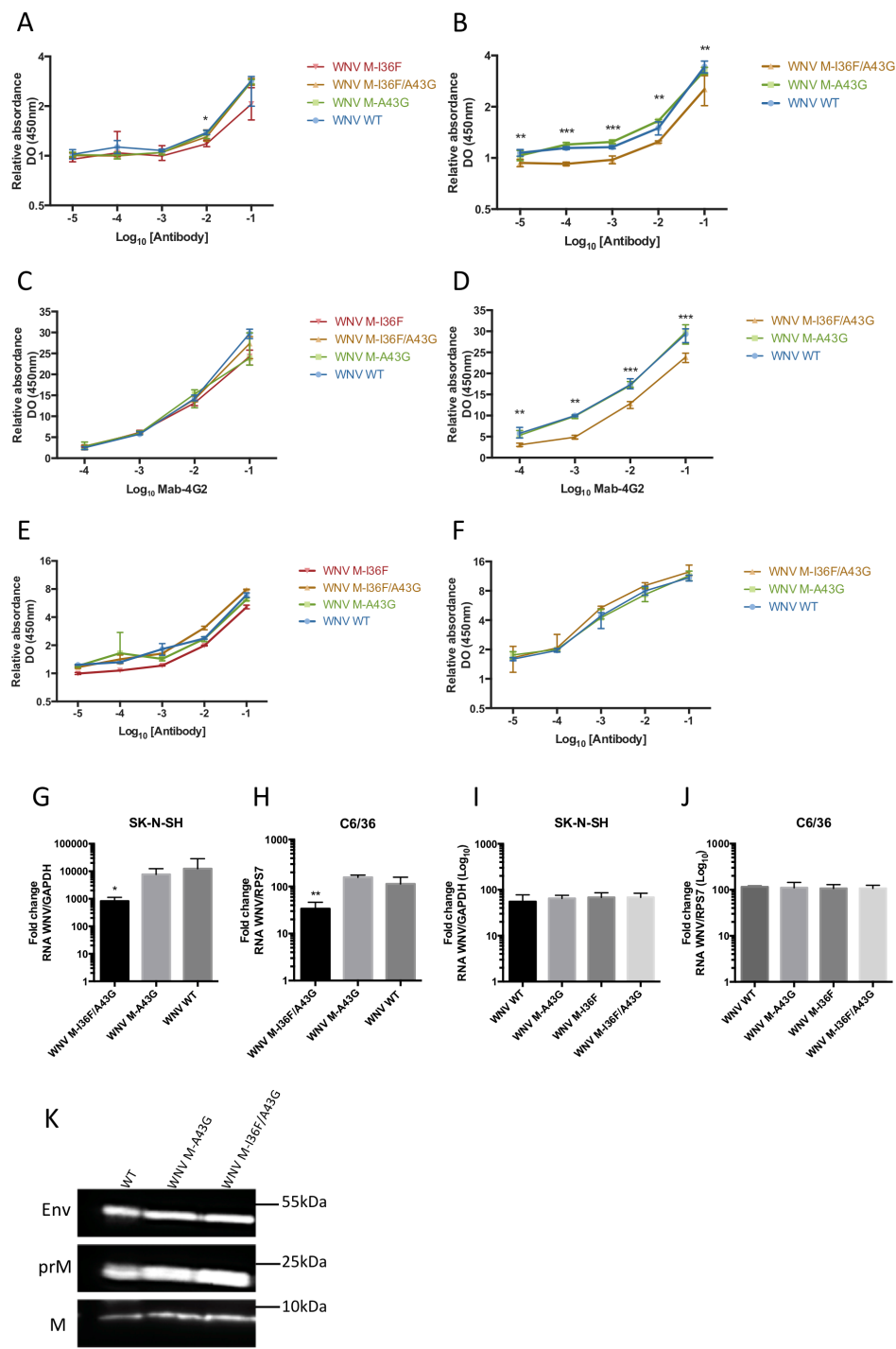


Figure 6:

